SUBMITTED TO THE ASTROPHYSICAL JOURNAL
Preprint typeset using LaTeX style emulateapj v. 14/09/00

X-RAY SPECTROSCOPY OF THE ACCRETING MILLISECOND PULSAR XTE J0929−314 IN OUTBURST

ADRIENNE M. JUETT[1], DUNCAN K. GALLOWAY, AND DEEPTO CHAKRABARTY[1,2]
Center for Space Research, Massachusetts Institute of Technology, Cambridge, MA 02139;
ajuett, duncan, deepto@space.mit.edu
Submitted to the Astrophysical Journal

ABSTRACT

We present the high-resolution spectrum of the accretion-powered millisecond pulsar XTE J0929−314 during its 2002 outburst, measured using the Low Energy Transmission Grating Spectrometer onboard the *Chandra X-ray Observatory*. The *Chandra* spectrum is well fit by a power-law + blackbody model with photon index Γ=1.55±0.03, blackbody temperature $kT_{\rm bb}$ = 0.65±0.03 keV, and blackbody normalization $R_{\rm bb,km}/d_{\rm 10kpc}$ = 7.6±0.8. No emission or absorption features are found in the high-resolution spectrum, with a 3σ equivalent width upper limit of 5 eV for most of the 1.5–25.3 Å wavelength range. The neutral absorption edges are consistent with the estimated interstellar absorption along the line of sight to the source. We found no orbital modulation of the 2–10 keV X-ray flux, to a 3σ upper limit of 1.1%, which implies an upper limit on the binary inclination angle of $i \lesssim 85^\circ$ for a Roche-lobe–filling companion. We also present the broadband spectrum measured over the course of the outburst by the *Rossi X-ray Timing Explorer* (*RXTE*). The *RXTE* spectrum of XTE J0929−314 is also well fit with a power-law + blackbody model, with average values of Γ = 1.76±0.03, $kT_{\rm bb}$ = 0.66±0.06 keV, and $R_{\rm bb,km}/d_{\rm 10kpc}$=5.9 ± 1.3. No significant evolution in the spectral shape was found over the course of the outburst. The blackbody temperature and normalization varied, but were anti-correlated such that the blackbody flux remained constant, with the power-law normalization strongly correlated to the (decreasing) flux of the source. We find that the difference in power-law photon indices measured from *Chandra* and *RXTE* spectra can be explained by a change in the power-law photon index at low energies, $E \lesssim 4$ keV, and that the combined spectrum is better fit by a either a Comptonization + blackbody model or a broken power-law + blackbody model.

Subject headings: binaries: close — stars: neutron — pulsars: individual (XTE J0929−314) — X-rays: binaries

1. INTRODUCTION

Millisecond pulsars (MSPs) have long been considered one of the possible endpoints of low-mass X-ray binary (LMXB) evolution. The neutron star (NS) is thought to be spun-up to a millisecond period by accretion from its low-mass companion. After the accretion phase has ended, the NS may turn on as a radio MSP. In the last five years, this theory has been confirmed with the identification of three accretion-powered MSPs, SAX J1808.4−3658, XTE J1751−305 and XTE J0929−314 (Wijnands & van der Klis 1998; Chakrabarty & Morgan 1998; Markwardt et al. 2002; Galloway et al. 2002).

Interestingly, all three accretion-powered MSPs are in short period binaries, with the two most recently discovered having binary periods ∼43 min (Markwardt et al. 2002; Galloway et al. 2002). These short periods place the MSPs XTE J1751−305 and XTE J0929−314 in the class of ultracompact binaries, defined as having orbital periods $\lesssim$80 min. Ultracompact binaries require hydrogen-deficient or degenerate donors (Nelson, Rappaport, & Joss 1986). Recently, O and Ne emission and absorption features were discovered in two known and three suspected ultracompact systems (Schulz et al. 2001; Juett, Psaltis, & Chakrabarty 2001; Juett & Chakrabarty 2002). These results led the authors to conclude that the donor stars are degenerate C-O WDs. On the other hand, the *XMM-Newton* spectrum of XTE J1751−305 did not show emission or absorption features (Miller et al. 2002). In addition, no unusual abundances were required to fit the neutral absorption edges. This result is consistent with the suggestion of Markwardt et al. (2002) that the donor in XTE J1751−305 is a He WD.

XTE J0929−314 was discovered in April 2002 by the All Sky Monitor onboard the *Rossi X-ray Timing Explorer* (*RXTE*; Remillard 2002). After its initial detection, in which 185 Hz pulsations were found, further *RXTE* observations exhibited Doppler shifts consistent with a 43.6-min binary orbit (Remillard, Swank, & Strohmayer 2002; Galloway et al. 2002). Radio and optical counterparts with positions consistent with the *Chandra* position were also detected (Rupen, Dhawan, & Mioduszewski 2002; Greenhill, Giles, & Hill 2002; Cacella 2002). An optical spectrum of XTE J0929−314 revealed emission lines from C III/N III λ4640-4650 and Hα λ6563 (Castro-Tirado et al. 2002). Given the optical detection of emission lines, and the ultracompact nature and high-Galactic latitude of the source, XTE J0929−314 is an ideal candidate for a high-resolution X-ray spectroscopic study to search for emission and absorption features similar to those seen in other ultracompact systems. In this letter, we present results from a Director's Discretionary Time observation of XTE J0929−314 with the *Chandra X-ray Observatory*, as well as spectral results from the *RXTE* pointed observations throughout the outburst.

2. OBSERVATION AND DATA REDUCTION

The 2002 outburst of XTE J0929−314 began around MJD 52370 and peaked at ≈ 31 mCrab (2–10 keV) on MJD 52394 (Galloway et al. 2002). The pointed *RXTE* observations commenced 2 d later, and proceeded once every few days through MJD 52456. The source dropped below the 3σ detection limit of 7.5×10^{-12} erg cm^{-2} s^{-1} (2–10 keV; equivalent to 0.32 mCrab) after MJD 52443.

[1] Also at Department of Physics, Massachusetts Institute of Technology
[2] Alfred P. Sloan Research Fellow

XTE J0929−314 was observed throughout its 2002 outburst by the two pointed instruments onboard *RXTE*. The Proportional Counter Array (PCA; Jahoda et al. 1996) aboard *RXTE* consists of five gas-filled proportional counter units (PCUs) with a total effective area of ≈ 6000 cm^2, sensitive to X-ray photons in the 2.5–60 keV range. The two instrument clusters comprising the High-Energy X-ray Timing Experiment (HEXTE; Gruber et al. 1996) present an effective area of ≈ 1600 cm^2 to photons in the energy range 15–250 keV. We extracted average spectra from standard instrument mode data ("Standard-2" and "Archive" for PCA and HEXTE, respectively) from each PCU/cluster for each observation. Since the instrumental gain is known to vary between PCUs, and also with time, we generated a separate response matrix for each PCU and each observation using PCARSP version 8.0, supplied with LHEASOFT version 5.2. We estimated background spectra using the "combined" gain epoch 5 (beginning 2000 May 13) faint-source model as input to PCABACKEST version 3.0. Over the course of the outburst, we collected 38 observations of XTE J0929−314 totaling 123.5 ks.

We also observed XTE J0929−314 with *Chandra* on 2002 May 15 (MJD 52409) for 18 ks using the Low Energy Transmission Grating Spectrometer (LETGS) and the Advanced CCD Imaging Spectrometer (ACIS; Weisskopf et al. 2002). The LETGS spectra are imaged by ACIS, an array of six CCD detectors. The LETGS/ACIS combination provides both an undispersed (zeroth order) image and dispersed spectra from the grating with a wavelength range of 1.4–63 Å and a spectral resolution of $\Delta\lambda = 0.05$ Å. The various orders overlap and are sorted using the intrinsic energy resolution of the ACIS CCDs. The observation used a Y-offset of $+1\farcm5$ in order to place the O K absorption edge on the back-side illuminated S3 CCD, which has suffered less degradation than the front-side illuminated CCDs.

Using `tgdetect`, we determined the zeroth order source position of XTE J0929−314 to be: R.A.=$09^{\rm h}29^{\rm m}20\fs15$ and Dec=$-31\arcdeg23\arcmin04\farcs3$, equinox J2000.0 (90% confidence error of $0\farcs6$[3]). The *Chandra* position is consistent with both the optical and radio counterpart positions (Rupen et al. 2002; Greenhill et al. 2002; Cacella 2002). The first order dispersed spectrum of XTE J0929−314 had an average count rate of 7.64 ± 0.02 cts s^{-1}. We examined the total count rate, as well as the count rates in two different energy ranges, to check for changes in the spectral state. We found no evidence for any change of state during the *Chandra* observation.

The "level 1" event file was processed using the CIAO v2.2 data analysis package[4]. The standard CIAO spectral reduction procedure was performed. We filtered the event file retaining those events tagged as afterglow events by the `acis_detect_afterglow` tool. Since order-sorting of grating spectra provides efficient rejection of background events, the afterglow detection tool is not necessary to detect cosmic ray afterglow events. No features were found that might be attributable to afterglow events.

For bright sources, pileup can be a problem for CCD detectors (see, e.g., Davis 2002). The zeroth order *Chandra* spectra of XTE J0929−314 was heavily affected by pileup and was not used in this analysis. In addition, it was found that the first order spectrum of XTE J0929−314 suffered from pileup in the range 5–12 Å (1–2.5 keV). In order to use the grating pileup kernel in ISIS, we created ARFs for each chip using the CIAO tool `mkgarf` and then combined them to create +1 and −1 order ARFs using a custom tool developed by J. Davis of the HETGS instrument team. (This tool is similar to the standard CIAO tool but correctly calculates the fractional exposure at each response bin.) The grating pileup kernel models the effect of pileup on grating spectra, similar to the pileup model available for CCD spectra in ISIS and XSPEC (see, Davis 2002, for a discussion of grating pileup modeling). In addition, the data and responses were rebinned to 0.083 Å to reflect the size of an ACIS event detection cell (3 CCD pixels). Background spectra were extracted from the standard LETG background regions. Spectral analysis of the *Chandra* observation of XTE J0929−314 was performed using ISIS (Davis 2002; Houck & DeNicola 2000).

3. SEARCHING FOR ORBITAL MODULATION

The presence (or absence) of orbital modulation of the X-ray flux can help constrain the inclination of the binary, and in turn the mass of the companion. Galloway et al. (2002) determined the orbital period of XTE J0929−314 to be 43.6 min from the Doppler modulation of the pulse arrival times. We searched both the *RXTE* and *Chandra* data for orbital modulation of the X-ray flux.

For the *RXTE* analysis, we calculated background-subtracted, solar-system barycenter corrected, 16-s binned lightcurves for each observation from photons in the energy range 3–13 keV. This range was selected to maximize the signal-to-noise ratio, and is identical to that used for the pulse timing analysis of Galloway et al. (2002). For each observation, we created a phase folded lightcurve of 8 bins using the measured orbital parameters, with phase zero set to the epoch of 90° mean longitude, $T_{\pi/2}$. The length of each observation was short compared to the decay timescale of the X-ray flux of XTE J0929−314, so it was not necessary to correct for the decline in X-ray flux during a single observation. Each lightcurve was then fit with a sine curve with variable amplitude and phase. From these results, we place a 3σ upper limit on the fractional rms modulation of 1.1%.

We also searched the *Chandra* data for orbital modulation of the X-ray flux. For the *Chandra* analysis, we first barycentered and randomized the first order grating events. Randomizing of the event arrival times consists of adding a random quantity uniformly distributed between 0–3.2 s, in order to avoid aliasing caused by the readout time. We calculated the phase of each first order event using the orbital parameters from Galloway et al. (2002) and created a 8 bin phase-folded lightcurve. We found an upper limit of 2.3% rms, consistent with the *RXTE* results.

Since the *Chandra* data is not subject to time gaps due to spacecraft motion, we calculated a Fourier transform of the first order events which had been made into a 10-s binned lightcurve. We searched for modulations of the X-ray flux with frequencies between 6×10^{-5} and 5×10^{-2} Hz. We found no evidence for any periodic modulation, with a 90%-confidence upper limit of 1.4% for the fractional rms amplitude over the frequency range. The 90%-confidence upper limit for the fractional rms amplitude of a signal at the orbital period is 0.4%, well within the upper limits given by the phase folding analyses.

[3] See http://asc.harvard.edu/cal/ASPECT/celmon/index.html

[4] http://asc.harvard.edu/ciao/

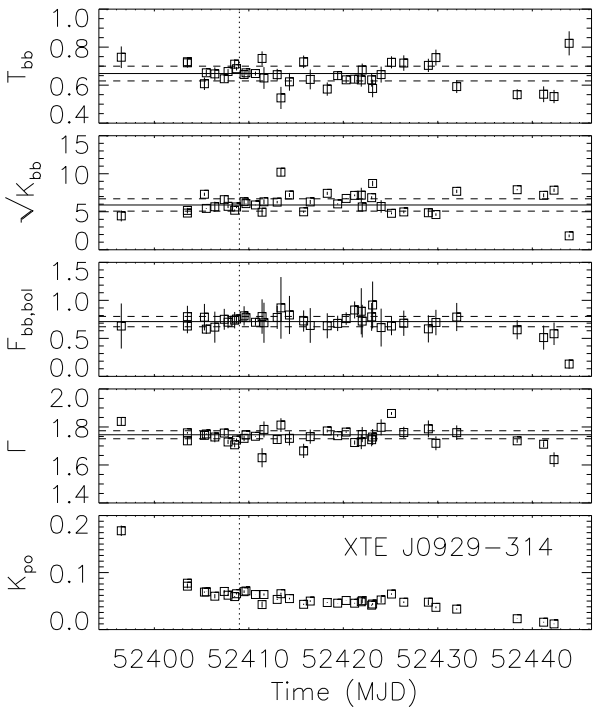

FIG. 1.— Spectral fit parameters derived from fitting an absorbed blackbody + power-law model to *RXTE* observations of XTE J0929−314. The panels, from top to bottom, show the blackbody temperature T_{bb} in keV; the blackbody normalization (= R_{km}/d_{10kpc}), estimated bolometric flux of the blackbody component (10^{-10} erg cm^{-2} s^{-1}), power-law photon index Γ, and power-law normalization (photons keV^{-1} cm^{-2} s^{-1} at 1 keV). The solid line shows the weighted mean over all the observations, while the dashed line shows the $\pm 1\sigma$ limits. The dotted line shows the time of the *Chandra* observation. Error bars show the 1-σ uncertainties.

4. SPECTRAL ANALYSIS

4.1. RXTE *Spectral Analysis*

We fitted the combined PCA and HEXTE spectra with a range of models which typically give good fits for other X-ray pulsars, including broken and cutoff power laws and analytical Comptonization approximations. There was no evidence for a high-energy spectral cutoff within the energy range in which the source was detected (typically $\lesssim 50$ keV). We did however measure significant residuals below 10 keV. These residuals could be minimized by adopting a broken power law model where the spectral index decreased by $\sim 10\%$ (i.e. the spectrum became harder) above 7 keV, or by adding a blackbody component with $kT_{bb} \sim 0.5$ keV to the power law. While both these models gave fits of similar quality, we rejected the former as unphysical and instead adopted the latter for the remainder of the *RXTE* fits.

We also included a multiplicative component to take into account the attenuation by intervening (neutral) material with cosmic abundances. The equivalent hydrogen column density N_H exhibited no significant variations between observations, and in the mean was $\sim 10^{21}$ cm^{-2}, consistent with the line-of-sight values interpolated from dust and H I maps (7.6×10^{20} and 10^{21} cm^{-2} respectively; Schlegel, Finkbeiner, & Davis 1998; Dickey & Lockman 1990). For consistency with the fits to *Chandra* data, we froze the N_H value in subsequent fits at 7.6×10^{20} cm^{-2}. The mean value of the reduced-χ^2 (= χ^2_ν) for power law and blackbody fits to spectra from all the observations was 1.04. While the worst-fitting observation gave a $\chi^2_\nu = 2.44$, the largest residuals arose from variations between PCUs (particularly at the lower energy bound) rather than any broad trend with energy. By excluding these lowest channels from the fit, and assuming a systematic error of 1%, we were able to reduce the fit statistic for that observation to $\chi^2_\nu = 1.30$.

The weighted mean of the blackbody temperature, kT_{bb}, was 0.66 ± 0.06 keV, while the normalization $\sqrt{K_{bb}} = R_{bb,km}/d_{10kpc} = 5.9 \pm 1.3$ (all errors are quoted at 90-% confidence unless otherwise noted). Both parameters showed significant variations during the outburst; however, they were significantly anticorrelated, so that the estimated bolometric blackbody flux ($\propto K_{bb} T_{bb}^4$) remained constant to within our measurement uncertainties ($\chi^2_\nu = 1.06$, see Figure 1). In the first observation, the blackbody component comprises only 3% of the flux in the 2–60 keV band, whereas in the last observation where significant blackbody and power-law components were detected, the blackbody accounted for 16% of the flux.

We calculated a weighted mean photon index of $\Gamma = 1.76 \pm 0.03$. The principal source of flux variation was the normalization of the power-law component (see Figure 1). While all parameters exhibited variations throughout the outburst, the power-law normalization was the only parameter to show a significant correlation with the integrated 2–10 keV flux (Spearman's rank correlation coefficient $\rho = 0.908$, equivalent to 5.4σ; Press et al. 1992). A power-law component was not significantly detected in the last observation on MJD 52443. A blackbody-only fit for that day exhibits a significantly (6.6σ) lower integrated blackbody flux than the weighted mean level for the previous observations. We did not detect XTE J0929−314 in subsequent observations (3σ upper limit on the flux of 7.5×10^{-12} erg cm^{-2} s^{-1}, 2–10 keV).

4.2. Chandra *Spectral Analysis*

We fit the *Chandra* spectrum with a power-law + blackbody model including absorption. The $+1.'5$ Y-offset in the observational setup allows for the entire 1.5–25.3 Å (0.5–8.3 keV) +1 order spectrum to be imaged on the S3 CCD. This CCD is backside-illuminated and has suffered less degradation than the front-side illuminated CCDs. Because of this and the lack of counts above 25 Å, we performed our spectral fits on only the +1 order spectrum in the range 1.5–25.3 Å.

Of the three known X-ray MSPs, XTE J0929−314 has the highest Galactic latitude and, probably the smallest interstellar column density along the line of sight to the source. Our *Chandra* observation allows for a direct determination of the strength of the absorption edges, in particular the O K edge and the Fe L triplet. To account for absorption and measure the optical depths of the edges, we used the `tbvarabs` absorption model (see, Wilms, Allen, & McCray 2000) with O and Fe abundances set to zero and the N_H fixed to 7.6×10^{20} cm^{-2}, the hydrogen column from dust maps (Schlegel et al. 1998). The O edge was fit with an `edge` model while the Fe L edges were fit using a custom model that employs the optical constant measurements of Kortright & Kim (2000). In addition, the C abundance in `tbvarabs` was allowed to vary in order to account for the known instrumental contamination of the ACIS CCDs[5]. We also included gaussian lines to fit the interstellar atomic O absorption line at 23.5 Å and the absorption feature at 23.36 Å, attributed to a 1s-2p transition in Fe_2O_3 (see, Schulz et al. 2002).

[5] For more information see, http://cxc.harvard.edu/cal/Links/Acis/acis/Cal_prods/qeDeg/index.html

We found a best-fit photon index of 1.55±0.03, with a normalization of (4.04±0.15)×10^{-2} photons keV^{-1} cm^{-2} s^{-1} at

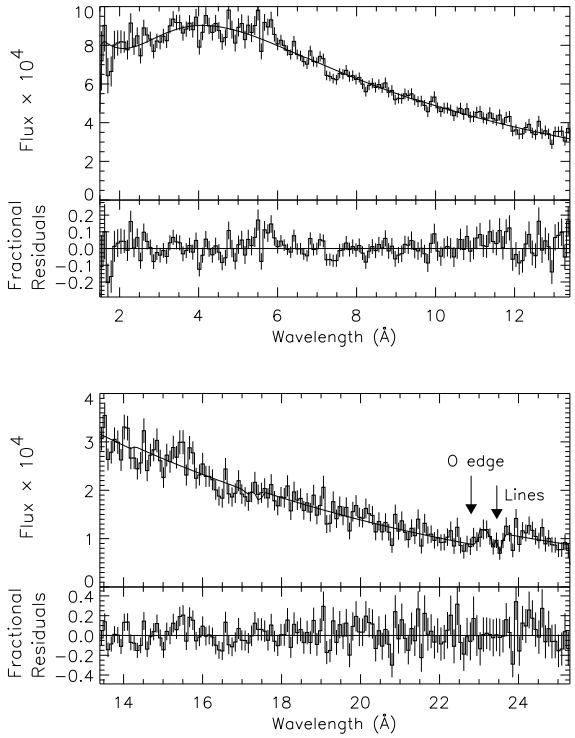

FIG. 2.— (*upper panels*) *Chandra* LETG +1 order flux spectrum (in units of photons cm^{-2} s^{-1} Å^{-1}) of XTE J0929–314 with best-fit power-law + blackbody model with absorption. The arrows indicate the positions of the O edge, and the atomic O and Fe_2O_3 absorption lines. (*lower panels*) Fractional residuals ([data−model]/model) of the LETG spectral fit shown above. The absorption models are consistent with the predicted interstellar absorption from dust maps.

1 keV. The *Chandra* best-fit blackbody temperature was $kT_{\rm bb}$ = 0.65 ± 0.03 keV, with $R_{\rm bb,km}/d_{\rm 10kpc}$ = 7.6 ± 0.8. Our best-fit model had a χ^2_ν = 1.001 and an unabsorbed 2–10 keV flux of 2.7×10^{-10} erg cm^{-2} s^{-1}.

The best-fit optical depth for O was 0.34±0.07, which translates to an equivalent hydrogen column density of (1.2±0.3)×10^{21} cm^{-2}, using the cross-section of Verner et al. (1993) and the O ISM abundance of Wilms et al. (2000). Although this is somewhat higher than the measured hydrogen column from dust maps, an instrumental contribution to the O edge has been reported[5], with an optical depth of ≈0.082. This contribution would add $N_{\rm H} \approx 0.3 \times 10^{21}$ cm^{-2} to the expected value, making the *Chandra* O edge measurement compatible with the dust map measurement. The best-fit line wavelength and flux of the atomic O absorption line were 23.52±0.06 Å and $(-1.46^{+0.7}_{-0.14}) \times 10^{-4}$ photons cm^{-2} s^{-1}; while the Fe_2O_3 absorption line is not significantly detected. The Fe-L edges were also not significantly detected, with an upper limit on the Fe column density of 3×10^{16} cm^{-2}, equivalent to an $N_{\rm H}$ = 1.1×10^{21} cm^{-2}, also consistent with the dust map measurement. The best-fit C abundance was $7.8^{+1.2}_{-0.7}$ times the interstellar C/H ratio of Wilms et al. (2000). This is slightly lower than the expected instrumental + interstellar contribution of 9.9±0.5 times the interstellar ratio. The instrumental edge depths for C and O were estimated using the recent calibration results presented at the *Chandra X-ray Center* website[5].

Besides the interstellar O absorption line, there were no prominent emission or absorption lines in the high-resolution spectrum of XTE J0929–314 (see Figure 2). We performed a careful search of the *Chandra* spectral residuals to place limits on the presence of any spectral features. Gaussian models with fixed FWHM = 2000 km s^{-1} were fit at each point in the wavelength range 1.5–25.3 Å. From this, we can place a 3σ limit of < 5 eV in the range 3.0–25.3 Å on the equivalent width (EW) of any line feature, either emission or absorption. The EW limit at $\lambda < 3$ Å is greater but below 35 eV. The 3σ flux limit on any line in the 1.5–25.3 Å range is $< 8 \times 10^{-5}$ photons cm^{-2} s^{-1}.

Our measured C abundance depends on the assumed continuum model, since the edge depth can not be directly measured (the C edge at 43 Å is outside our bandpass). In order to test if the C abundance was the cause of the difference in the photon index between the *Chandra* and *RXTE* fits, we refit the *Chandra* spectrum with a fixed C abundance of 9.9 times the interstellar C/H ratio. With the C abundance fixed, the best-fit photon index was 1.62±0.03. This is still significantly different from the best-fit photon index found in the *RXTE* spectra. The best-fit power-law normalization increased to (4.50±0.07)×10^{-2} photons keV^{-1} cm^{-2} s^{-1}. The other fit parameters were consistent with the previous fit within errors. We also considered the possibility that the pileup model was giving rise to the lower photon index in the *Chandra* spectral fits. When the *Chandra* data is fit without the pileup model, and excluding the piled-up region (1–3 keV) of the spectrum, we find spectral parameters consistent with the results found using the pileup model.

5. COMBINED *Chandra* AND *RXTE* SPECTRAL FITS

To investigate the difference in the spectral results between *Chandra* and *RXTE*, we performed combined spectral fits with the *Chandra* and *RXTE* data. A single *RXTE* observation (70096-03-05-00) taken within a few hours of the *Chandra* data was used to represent the *RXTE* spectrum of XTE J0929–314. To simplify fitting, the piled-up region (1-3 keV) of the *Chandra* data was excluded and the pileup kernel was not used. The combined data was fit with a blackbody + either a power-law, broken power-law or the `compTT` model which describes Comptonization of soft photons by a hot plasma (Titarchuk 1994). The broken power-law and Comptonization models allow for turnover at low energies which could explain the difference in the *Chandra* and *RXTE* spectral results. The absorption was described by the `tbvarabs` model with the C abundance allowed to vary for the *Chandra* observation only, while best-fit edge depths from the *Chandra* analysis were used for the O and Fe edges. We also included a gaussian line, fixed to the best-fit *Chandra* value, to model the atomic O absorption at 23.5 Å. Multiplicative constants were included to compensate for any instrumental normalization differences. We find that the normalizations of the PCA spectra are ≈20% larger than for *Chandra*, while the HEXTE spectra are ≈20% lower. Similar normalization differences have been noted before (see, Kuulkers et al. 2002, and references therein).

As a check on the instrumental calibrations, we directly compared the *Chandra* and *RXTE* data in the same energy range by fitting the high energy (3–8 keV) *Chandra* data, in conjunction with the *RXTE* data, to an absorbed power-law + blackbody model with absorption fixed to $N_{\rm H} = 7.6 \times 10^{20}$ cm^{-2}. The fits are consistent with the results of the *RXTE* data, Γ = 1.74±0.02, $kT_{\rm bb}$ = 0.66±0.03 keV, and $R_{\rm bb,km}/d_{\rm 10kpc}$ = 5.9 ± 0.7, with

$\chi^2_\nu = 1.03$.

We then fit the full *Chandra* and *RXTE* spectra with a power-law + blackbody model. When the edge parameters were fixed to the *Chandra* best-fit values, the photon index had a best-fit value of 1.628±0.009 and with a $\chi^2_\nu = 1.20$ (see Table 1). We note that the χ^2_ν of the power-law + blackbody fit to the *RXTE* data alone was 1.06. If we fix the C abundance to the expected value of 9.9 times the interstellar C/H ratio, the photon index increases to 1.656±0.009 ($\chi^2_\nu = 1.14$). If we instead allow the C abundance to vary, the best-fit photon index increases to 1.72±0.02 ($\chi^2_\nu = 1.09$), giving a photon index consistent with the *RXTE* spectral results, but with a C abundance of 14.1±1.2 times the interstellar C/H ratio. This value is inconsistent with the estimate of the C abundance from instrument calibration work (see §4.2). As can be seen, the continuum spectral parameters are highly dependent on the assumed absorption.

We performed the same fits using the `comptt` in place of the power-law component. The Comptonization model provides for a low-energy turnover in the spectrum. The electron temperature was fixed to 50 keV, the upper limit of the energy range. In addition, we used a spherical geometry in order to compare with the spectral fit of SAX J1808.4–3658 (Titarchuk et al. 2002). The `comptt` model provides a better fit to the data compared with the power-law ($\chi^2_\nu = 1.09$–1.07, see Table 1). We performed an F-test to formally compare the two models and found that in all cases the Comptonization model was better with the a significance $> 99\%$. For the two fixed values of the C abundance, the results of the `comptt` + blackbody fits are consistent within error with a seed photon temperature, $kT_0 \approx 0.13$ keV and optical depth, $\tau_p \approx 2.7$. When the C abundance is allowed to vary, the fit improves but becomes inconsistent with the other results, which is probably due to degeneracy between the parameters.

In the best-fit the `comptt` + blackbody model, the blackbody component has parameter values of $kT_{\rm bb} = 0.71$ keV and $R_{\rm bb,km}/d_{\rm 10kpc} = 5.5$. These values are consistent with the power-law fits both to the combined data and with the blackbody parameters from each instrument fit, indicating that the blackbody temperature and flux are independent of the exact continuum model used. We find $kT_0 < kT_{\rm bb}$, similar to the fit of SAX J1808.4–3658 using the same model (Titarchuk et al. 2002). We note that the `comptt` model is in itself an approximation to a full treatment of Comptonization, in particular at soft energies. If we assume that the blackbody provides the input photons to the Comptonization component, then we would expect $kT_0 = kT_{\rm bb}$. We fit the data with the constraint $kT_0 = kT_{\rm bb}$, but the fit was unreasonable with $\chi^2_\nu > 2.0$. Interestingly, Gierliński et al. (2002) used a different Comptonization model and found $kT_0 = kT_{\rm bb}$ in spectral fits of SAX J1808.4–3658. We employed the same model to fit XTE J0929−314 (`compPS`, Poutanen & Svensson 1996), but found similar values for the input photon temperature and optical depth as found using the `comptt` model.

We also fit the data with a broken power-law + blackbody model to test for low-energy turnover without relying on the assumptions inherent in the Comptonization model. We find that the data is also well fit ($\chi^2_\nu = 1.08$) by a broken power-law + blackbody model with $\Gamma_1 = 1.26$–1.56, $\Gamma_2 = 1.75$, and $E_{\rm break} = 1.4$–4.4 keV, and blackbody parameters consistent with previous fits (see Table 1).

6. DISCUSSION

The broadband X-ray spectra of the three millisecond X-ray pulsars discovered to date are all similar, comprising a blackbody component with $kT_{\rm bb} = 0.5$–1 keV, and a power law with photon index $\Gamma = 1.4$–1.8, possibly with a spectral cutoff above 40 keV or so (Gierliński et al. 2002; Markwardt et al. 2002; Miller et al. 2002; Galloway et al. 2002). These components are generally attributed to a "hot spot" on the surface of the neutron star and a shock-heated accretion column, respectively. From our fits, we find a blackbody radius of $R_{\rm bb,km} = (5.3-7.7)\, d_{\rm 10kpc}$. Given the lower limit on the distance of 5 kpc (Galloway et al. 2002), we find a lower limit on the radius of $R_{\rm bb} > 2.7$ km. We note that this lower limit does not include a correction for the conversion between the color temperature and the effective temperature of the neutron star atmosphere (see, Lewin, van Paradijs, & Taam 1993, for a discussion). This correction could increase the inferred radius by a factor of ≈ 2. The inferred radius may imply the existence of a "hot spot" emission region for the blackbody component, but further analysis is required before such a claim can be justified.

TABLE 1
COMBINED *Chandra* AND *RXTE* SPECTRAL FITS[a]

Model	Carbon Abundance[b]	Γ_1/kT_0 /keV	$E_{\rm break}$ keV	Γ_2/τ	A[c]	$kT_{\rm bb}$ keV	$R^2_{\rm km}/d^2_{\rm 10kpc}$	χ^2/dof
PL	7.8 (fix)	1.628±0.009	···	···	4.58±0.07	0.730±0.015	28±3	1006/837
PL	9.9 (fix)	1.656±0.009	···	···	4.90±0.08	0.717±0.016	28±3	950/837
PL	14.1±1.2	1.72±0.02	···	···	5.7±0.3	0.68±0.02	31±5	904/833
Comp	7.8 (fix)	0.144±0.009	···	2.72±0.06	3.21±0.09	0.709±0.016	29±3	911/836
Comp	9.9 (fix)	0.125±0.014	···	2.69±0.06	3.6±0.2	0.707±0.017	30±4	906/836
Comp	13.2±1.2	$0.07^{+0.04}_{-7}$	···	2.55±0.07	$5.8^{+7.5}_{-1.8}$	0.67±0.02	34±5	894/832
BKN PL	7.8 (fix)	1.26±0.09	1.4±0.3	1.74±0.02	5.06±0.19	0.66±0.03	34±8	900/835
BKN PL	9.9 (fix)	1.56±0.03	4.4±0.9	1.75±0.02	4.67±0.17	0.61±0.03	60±30	897/835

[a] All errors are quoted at the 90%-confidence level

[b] Carbon abundance ratio relative to ISM, $(C/H)/(C/H)_{\rm ISM}$

[c] Power-law and broken power-law normalization at 1 keV in units of 10^{-2} photons keV^{-1} cm^{-2} s^{-1}. Comptonization normalization in units of 10^{-3}.

As with the other two accreting millisecond pulsars, little spectral evolution is seen throughout the outburst of XTE J0929−314. The blackbody component parameters vary significantly, but are anticorrelated such that the estimated bolometric flux of this component is constant. This is in contrast with the behavior of SAX J1808.4−3658, in which both the blackbody normalization and temperature were found to decrease throughout the outburst, along with the hard component normalization (Gierliński et al. 2002).

We find that the spectrum is well described by a power-law + blackbody model over limited energy ranges, with interstellar absorption consistent with $N_{\rm H} = 7.6 \times 10^{20}$ cm^{-2} the expected hydrogen column density along the line of sight to the source. The *Chandra* spectrum shows no prominent emission or absorption lines in the spectrum (similar to XTE J1751−305; Miller et al. 2002), with an EW limit of < 5 eV for much of the spectral range and a line flux limit of $< 8 \times 10^{-5}$ photons cm^{-2} s^{-1}. No orbital modulation of the X-ray flux was detected in either the *Chandra* or *RXTE* data. From the lack of dips or eclipses, we can set an upper limit on the binary inclination of $i \lesssim 85^{\circ}$ for a Roche-lobe–filling companion.

We find that the best-fit photon index is significantly different between the *Chandra* and *RXTE* fits with $\Gamma = 1.55 - 1.62$ for the *Chandra* fits, dependent on the assumed instrumental C abundance, and $\Gamma = 1.76$ for the *RXTE* fits. The difference in the photon index between the *Chandra* and *RXTE* spectral fits is similar to that noted by Miller et al. (2002) between the *RXTE* and *XMM* spectral fits of XTE J1751−305. From their *XMM* EPIC spectrum, Miller et al. (2002) found a best-fit power-law photon index of 1.44, while Markwardt et al. (2002) found a best-fit photon index of 1.7–1.9 using *RXTE*.

We suggest that this difference arises from spectral turnover at low energies. While a power-law model is a reasonable approximation to Comptonization at high energies, extrapolating the power law to low energies leads to a predicted flux that diverges at zero energy. Thermodynamics therefore requires that the power-law spectrum turn over at low energies (see, e.g., Psaltis 1998). Previous X-ray instruments have generally not required low energy turnovers for two reasons: low spectral resolution and limited bandpasses. In low-resolution fits of LMXBs, the interstellar absorption component can generally be used to compensate for possible deviations from a power law at low energies. The high-resolution capabilities of *Chandra* and *XMM* allow for a direct measurement of the edge depths and thus the column density to the source, effectively constraining one of the free parameters in the continuum fits. Combining the high-resolution capabilities of *Chandra* and *XMM* with the broadband coverage of *RXTE* allows for more accurate descriptions of the continuum emission from LMXBs.

The combined *Chandra* and *RXTE* spectrum of XTE J0929−314 is well fit by either a Comptonization + blackbody model (which implicitly includes a low-energy turnover from the Comptonization component), or a broken power-law + blackbody model, with break energy 1.4–4.4 keV. The high-energy ($E > 3$ keV) *Chandra* spectrum is consistent with the *RXTE* spectral results, indicating that instrumental differences alone do not give rise to the spectral turnover. We reject the possibility that the pileup model causes the lower photon index in *Chandra*-only fits, since fits without the pileup model give consistent parameter values. In addition, the spectral fit of XTE J1751−305 using *XMM* provides independent support for the presence of low-energy turnover in the spectra of millisecond X-ray pulsars and suggests that this turnover is astrophysical in origin.

A Comptonization + blackbody model was also used to fit the *RXTE* spectrum of the millisecond X-ray pulsar SAX J1808.4−3658 in outburst (Titarchuk et al. 2002). These authors claim that the low ($\tau_0 \approx 4$) optical depth of the Comptonizing region allows for the pulsations of the NS to be detected, while the higher optical depths ($\tau_0 > 5$) reported in more luminous LMXBs suppress the pulsation amplitudes. We find a best-fit $\tau_0 \approx 2.7$ for XTE J0929−314, consistent with this explanation. However, we note that Miller et al. (2002) did not find an acceptable fit of the *XMM* spectra of the millisecond X-ray pulsar XTE J1751−305 using a Comptonization model.

Both the power-law and Comptonization models required the addition of a blackbody at $kT_{\rm bb} = 0.65 - 0.7$ keV. The similarity of the blackbody parameters in all of the fits, gives us confidence that the component is required and that the parameters can be reliably measured, even with the 2 keV lower energy limit of *RXTE*. In the Comptonization + blackbody fits, we find $kT_0 < kT_{\rm bb}$. Similar fits to the same *RXTE* data of SAX J1808.4−3658 reach different conclusions as to the best-fit values of kT_0 and $kT_{\rm bb}$. Titarchuk et al. (2002) found that $kT_0 < kT_{\rm bb}$, while Gierliński et al. (2002) found $kT_0 = kT_{\rm bb}$. Given that the kT_0 value found by Titarchuk et al. (2002) is well outside the *RXTE* spectral range, and that different Comptonization models were used in the fits, it is difficult to compare the SAX J1808.4−3658 results. On the other hand, the low energy range of *Chandra* allows us to make a more robust measurement of kT_0 for XTE J0929−314. The difference in the best-fit values of kT_0 and $kT_{\rm bb}$ in our fits, along with the constant blackbody flux during the outburst, suggests that the blackbody is not the input to the Comptonization, but is rather a separate component. Further analyses, including pulse-phase spectroscopy, could reveal more about the geometry of the system and the origin of the emission components.

We would like to thank *Chandra* Director Harvey Tananbaum for approving our DDT observation. This research has made use of data obtained through the High Energy Astrophysics Science Archive Research Center Online Service, provided by the NASA/Goddard Space Flight Center. This work was supported in part by NASA under contracts NAS8-38249 and NAS8-01129 and grant NAG5-9184.

REFERENCES

Cacella, P. 2002, IAU Circ., No. 7893
Castro-Tirado, A. J., Caccianiga, A., Gorosabel, J., Kilmartin, P., Tristram, P., Yock, P., Sanchez-Fernandez, C., & Alcoholado-Feltstrom, M. E. 2002, IAU Circ., No. 7895
Chakrabarty, D. & Morgan, E. H. 1998, Nature, 394, 346
Davis, J. 2002, Proc. SPIE, submitted
Dickey, J. M. & Lockman, F. J. 1990, ARA&A, 28, 215
Galloway, D. K., Chakrabarty, D., Morgan, E. H., & Remillard, R. A. 2002, ApJ, 576, L137
Gierliński, M., Done, C., & Barret, D. 2002, MNRAS, 331, 141
Greenhill, J. G., Giles, A. B., & Hill, K. M. 2002, IAU Circ., No. 7889
Gruber, D. E., Blanco, P. R., Heindl, W. A., Pelling, M. R., Rothschild, R. E., & Hink, P. L. 1996, A&AS, 120, C641
Houck, J. C., & DeNicola, L. A. 2000, in ASP Conf. Ser. 216, Astronomical Data Analysis Software and Systems IX, ed. N. Manset, C. Veillet, & D. Crabtree (San Francisco: ASP), 591
Jahoda, K., Swank, J. H., Giles, A. B., Stark, M. J., Strohmayer, T., Zhang, W., & Morgan, E. H. 1996, Proc. SPIE, 2808, 59

Juett, A. M. & Chakrabarty, D. 2002, ApJ, submitted (astro-ph/0206417)
Juett, A. M., Psaltis, D., & Chakrabarty, D. 2001, ApJ, 560, L59
Kortright, J. B., & Kim, S.-K. 2000, Phys. Rev. B, 62, 12216
Kuulkers, E., den Hartog, P. R., in 't Zand, J. J. M., Verbunt, F. W. M., Harris, W. E., & Cocchi, M. 2002, A&A, submitted
Lewin, W. H. G., van Paradijs, J., & Taam, R. E. 1993, SSRv, 62, 223
Markwardt, C. B., Swank, J. H., Strohmayer, T. E., in 't Zand, J. J. M., & Marshall, F. E. 2002, ApJ, 575, L21
Miller, J. M., Wijnands, R., Méndez, M., Tiengo, A., van der Klis, M., Chakrabarty, D., Gaensler, B. M., & Lewin, W. H. G. 2002, ApJ, submitted (astro-ph/0208166)
Nelson, L. A., Rappaport, S. A., & Joss, P. C. 1986, ApJ, 304, 231
Poutanen, J. & Svensson, R., 1996, ApJ, 470, 249
Press, W. H., Teukolsky, S. A., Vetterling, W. T., & Flannery, B. P. 1992, Numerical recipes in FORTRAN. The art of scientific computing (2nd ed.; New York: Cambridge University Press)
Psaltis, D. 1998, Ph. D. Thesis, University of Illinois at Urbana-Champaign
Remillard, R. A. 2002, IAU Circ., No. 7893
Remillard, R. A., Swank, J., & Strohmayer, T. 2002, IAU Circ., No. 7893
Rupen, M. P., Dhawan, V., & Mioduszewski, A. J. 2002, IAU Circ., No. 7893
Schlegel, D. J., Finkbeiner, D. P., & Davis, M. 1998, ApJ, 500, 525
Schulz, N. S., Chakrabarty, D., Marshall, H. L., Canizares, C. R., Lee, J. C., & Houck, J. 2001, ApJ, 563, 941
Schulz, N. S., Cui, W., Canizares, C. R., Marshall, H. L., Lee, J. C., Miller, J. M., & Lewin, W. H. G. 2002, ApJ, 565, 1141
Titarchuk, L. 1994, ApJ, 434, 313
Titarchuk, L., Cui, W., & Wood, K. 2002, ApJ, 576, L49
Verner, D. A., Yakovlev, D. G., Band, I. M., & Trzhaskovskaya, M. B. 1993, Atomic Data & Nucl. Data Tables, 55, 233
Weisskopf, M. C., Brinkman, B., Canizares, C., Garmire, G., Murray, S., & van Speybroeck, L. P. 2002, PASP, 114, 1
Wijnands, R. & van der Klis, M. 1998, 394, 344
Wilms, J., Allen, A., & McCray, R. 2000, ApJ, 542, 914